ACS Catalysis

pubs.acs.org/acscatalysis

Research Article

Insight into the Nature of the ZnO_x Promoter during Methanol Synthesis

Remco Dalebout, Laura Barberis, Giorgio Totarella, Savannah J. Turner, Camille La Fontaine, Frank M. F. de Groot, Xavier Carrier, Ad M. J. van der Eerden, Florian Meirer, and Petra E. de Jongh*

Cite This: *ACS Catal.* 2022, 12, 6628−6639

Read Online

ACCESS | Metrics & More | Article Recommendations | Supporting Information

ABSTRACT: Despite the great commercial relevance of zinc-promoted copper catalysts for methanol synthesis, the nature of the Cu−ZnO_x synergy and the nature of the active Zn-based promoter species under industrially relevant conditions are still a topic of vivid debate. Detailed characterization of the chemical speciation of any promoter under high-pressure working conditions is challenging but specifically hampered by the large fraction of Zn spectator species bound to the oxidic catalyst support. We present the use of weakly interacting graphitic carbon supports as a tool to study the active speciation of the Zn promoter phase that is in close contact with the Cu nanoparticles using time-resolved X-ray absorption spectroscopy under working conditions. Without an oxidic support, much fewer Zn species need to be added for maximum catalyst activity. A 5−15 min exposure to 1 bar H_2 at 543 K only slightly reduces the Zn(II), but exposure for several hours to 20 bar H_2/CO and/or H_2/CO/CO_2 leads to an average Zn oxidation number of +(0.5−0.6), only slightly increasing to +0.8 in a 20 bar H_2/CO_2 feed. This means that most of the added Zn is in a zerovalent oxidation state during methanol synthesis conditions. The Zn average coordination number is 8, showing that this phase is not at the surface but surrounded by other metal atoms (whether Zn or Cu), and indicating that the Zn diffuses into the Cu nanoparticles under reaction conditions. The time scale of this process corresponds to that of the generally observed activation period for these catalysts. These results reveal the speciation of the relevant Zn promoter species under methanol synthesis conditions and, more generally, present the use of weakly interacting graphitic supports as an important strategy to avoid excessive spectator species, thereby allowing us to study the nature of relevant promoter species.

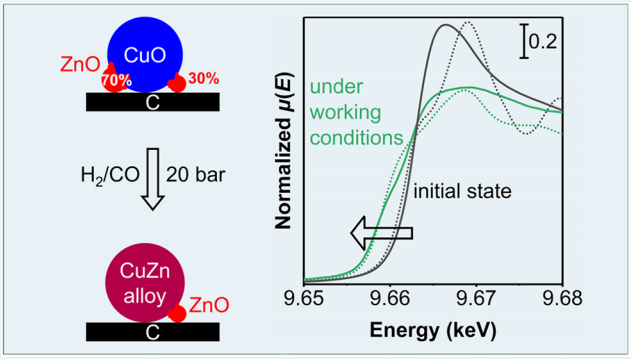

KEYWORDS: *methanol synthesis, CO hydrogenation, CO_2, zinc oxide promotion, carbon support, silica, X-ray absorption spectroscopy, copper nanoparticles*

1. INTRODUCTION

Methanol synthesis is an important, decades-old industrial process. Nowadays, a coprecipitated Cu/ZnO/Al_2O_3 catalyst is used to hydrogenate CO_2 to methanol in a CO-rich environment. It has been well established that the methanol is predominantly formed from CO_2 rather than from CO. The role of the CO is to supply CO_2 *via* the reaction with water, which also keeps the water level low.[1−6] Generally accepted is that Cu is the main active component where ZnO_x plays a crucial role in promoting the catalyst activity with about an order of magnitude.[5,7−11] Yet, the exact role of the ZnO_x promoter is still under debate,[12−14] especially due to a lack of detailed knowledge on the ZnO_x speciation, structure, and its interaction with Cu under the typical methanol synthesis conditions at 473−573 K and 20−100 bar.[15,16]

Various hypotheses exist to explain the role of the ZnO_x promotion. It has been suggested that ZnO_x increases the Cu dispersion and thereby the active Cu surface area[17,18] and that the promoter supplies hydrogen to the Cu surface by spillover.[19,20] The oxidation state of ZnO_x can also play a role in the morphological change of small Cu particles due to a varying degree of the Cu−ZnO_x interaction, thereby varying the exposed Cu surface planes.[21] However, by now it is broadly accepted that the coverage of Cu nanoparticles with partially reduced ZnO is essential for the enhanced methanol production. An open question is still whether the promotion is due to the formation of a ZnO_x layer on the Cu particles,[19,22−24] to the formation and migration of Zn atoms on (or into) the Cu surface,[10,13,25,26] or to the creation of active defects upon Cu−ZnO_x interaction.[19,23,27] Research is typically performed on catalysts supported on metal oxides, which may obscure the

Received: November 6, 2021
Revised: May 8, 2022
Published: May 20, 2022

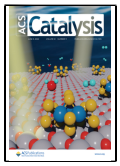

active ZnO_x phase by the formation of mixed Zn metal oxides and hence may significantly differ from the relevant speciation and distribution of the active fraction of the ZnO_x promoter.

It is generally accepted that ZnO_x (partially) covers the Cu nanoparticles in reducing conditions. The fractional coverage of Cu with ZnO_x during reaction conditions is mainly influenced by three factors: the feed composition, governing the degree of ZnO_x reduction; the ZnO_x loading; and the Cu particle size. For example, Kuld et al.[13] showed that by applying various feeds during catalyst activation an optimal Zn coverage over a Cu surface of 0.47 was achieved using a $Cu/ZnO/Al_2O_3$ catalyst of constant composition during CO/CO_2 hydrogenation at ambient pressure. Yet, contradictory results for the optimal Zn coverage were reported by varying the ZnO_x loading under different reaction conditions.[28,29] Also in a pure H_2/CO_2 feed, an optimal Zn coverage of 0.20, or an atomic Zn/Cu ratio of 1.2−1.6, was reported for Cu/ZnO catalysts.[19,22,23,30,31] The question remains what the actual state of the ZnO_x is during working conditions in different feeds at high pressure (e.g., H_2/CO feed), syngas enriched with a relevant amount of CO_2 (2−6 vol %[1−5]), or an H_2/CO_2 feed.

Much effort has been devoted to studying the interaction and oxidation state of ZnO_x species in CuZn-based catalysts in the calcined state[29,32−34] and before/after[33,35−39] or during[14,32,40−43] exposure to reducing atmospheres at (near-)ambient pressures (up to 8 bar). On the basis of those results, it is still inconclusive whether the oxidation state of ZnO_x slightly changes[35,36,40] and whether Cu−Zn alloys are formed[14,38,44] or not.[33,35,41,42] For example, recent studies reported the formation of a Cu−Zn alloy in a $Cu/ZnO/Al_2O_3$ catalyst during a $(CO_2/)H_2$ treatment at 15 bar and 533 K,[45] but this alloy formation was absent for a Cu/ZnO/faujasite catalyst with almost a 1-to-1 ratio of Cu and Zn.[46] A recently developed, unique tool that allows us to gain insight into the Zn oxidation state and speciation under realistic high-pressure conditions and in the working state is X-ray absorption spectroscopy (XAS). Very recently, Divins et al.[24] published an interesting *operando* study at 20−40 bar in a CO_2-enriched syngas feed using silica and alumina supports, ascribing the active ZnO_x speciation to a distorted ZnO_x phase with a maximum content of 9 at% Zn^0 atoms but most of the Zn species present as metal oxides.

A major obstacle to study the nature of the active site of the ZnO_x promoter is the strong interaction of the promoter with the oxidic catalyst support, which leads to the formation of a large fraction of Zn spectator species present as formates, oxides, or mixed metal phases.[24,37,45−49] Hence, the active promoter species represents only a fraction of the Zn species present in the system, and averaged information, such as the Zn oxidation state and coordination number, are not representative for the active ZnO_x promoter species.

We present graphitic carbon as a support with very limited interaction with Cu and ZnO_x.[47,48] In combination with a relatively low ZnO_x loading, it allows us to study specifically the ZnO_x in contact with the Cu nanoparticles during methanol synthesis and its speciation and interaction with the Cu, based on time-resolved XAS experiments under working conditions, also as a function of different feed compositions.

2. EXPERIMENTAL SECTION

2.1. Catalyst Synthesis. A series of $CuZnO_x/C$ catalysts, with similar Cu weight loadings (8.0 ± 0.4 wt %) but varying Zn/Cu molar ratios, were prepared *via* incipient wetness impregnation following a published method.[5] In brief, powdered high-surface-area graphite (TIMREX E-HSAG500, TIMCAL Graphite & Carbon) was dried at *ca.* 443 K under dynamic vacuum for 1.5 h. The support was impregnated at room temperature under static vacuum to 95% of the total pore volume with an acidified aqueous solution containing 1.8 M copper nitrate (Acros Organics, 99%) and 0−1.8 M zinc nitrate (Sigma-Aldrich, ≥99%). Subsequently, the impregnated support was dried overnight at room temperature under dynamic vacuum and further reduced at 503 K (ramp 2 K min^{-1}) in a 100 mL min^{-1} flow of 20 vol % H_2/N_2 for 2.5 h. After cooling to room temperature, the sample was exposed to a flow of 100 mL min^{-1} flow of 5 vol % O_2/N_2 for 1 h, heated to 473 K with a ramp of 1 K min^{-1} and oxidized at 473 K in 15 vol % O_2/N_2 for 1 h.

The Cu/C (8.1 wt % Cu), ZnO_x/C (9.9 wt % ZnO), and $CuZnO_x/SiO_2$ catalysts were synthesized following the same procedure as for the $CuZnO_x/C$ catalysts using the respective metal nitrate(s). A different heat treatment was applied only for the ZnO_x/SiO_2 catalyst (10.0 wt % ZnO): the dried impregnate was heated to 723 K (ramp 2 K min^{-1}) in a 200 mL min^{-1} g_{cat}^{-1} flow of 2 vol % NO/inert for 1 h.[50] Both SiO_2-based catalysts were supported on silica gel (25−75 μm, Davisil, grade 643, Sigma-Aldrich, ≥99%). All catalysts are named CuZn-*X*/C or CuZn-*X*/SiO_2, in which *X* represents the molar Zn/(Cu + Zn) ratio expressed as percentage and is based on the nominal loading. A commercial $Cu/ZnO/Al_2O_3/MgO$ catalyst from Alfa Aesar, containing a Cu/Zn/Al/Mg ratio of 63.8/24.8/10.1/1.3 wt %, served as a reference.

2.2. Catalyst Characterization. N_2 physisorption isotherms were recorded on a Micromeritics TriStar II Plus apparatus at 77 K. The samples were first dried at 443 K (or at 573 K for the SiO_2 support) under an N_2 flow overnight. The BET surface area was determined according to the IUPAC procedure.[51] A Barrett−Joyner−Halenda (BJH) analysis was applied to obtain pore size distributions, using either a carbon black or Harkins-Jura statistical thickness curve. The single-point total pore volume V_{tot} was determined at p/p_0 = 0.995. Integration of the differential pore size distribution (derived from the adsorption branch) between 2 and 50 nm yielded the mesoporosity. The micropore volume V_{micro} was calculated using the *t*-plot method.

Transmission electron microscopy (TEM) imaging was performed on an FEI Tecnai 20 apparatus, operating at 200 kV. High-angle, annular, dark-field scanning transmission electron microscopy (HAADF-STEM) images were obtained on a Thermo Fisher Scientific Talos F200X apparatus, operating at 200 kV. With the same apparatus, chemical maps were recorded using energy-dispersive X-ray (EDX) detectors. The EM samples for the carbon-supported catalysts were prepared by deposition of an ethanolic dispersion of the catalyst onto holey carbon film-coated Cu or Au grids (Agar, 300 mesh). As adequate TEM measurements on the silica-supported catalysts as such were not possible, they were ultramicrotomed. The catalysts were embedded in a two-component epoxy resin (Struers, EpoFix), which was heated overnight at 333 K and cut in 60−70 nm slices on a Leica Ultracut E. The slices were deposited on the aforementioned Au grids, which were made hydrophilic by glow discharge in a Cressington 208 carbon coater. At least 350 individual particles at various locations within the sample were measured to determine the number-averaged $Cu(Zn)O_x$ particle sizes (d_N) with the standard deviation (s_N) representing the width of the size distribution. These mean sizes were translated into surface-averaged particle sizes (d_S) *via*

https://doi.org/10.1021/acscatal.1c05101
ACS Catal. 2022, 12, 6628−6639

$d_S \pm s_S = \sqrt{\frac{1}{N}\sum_{i=1}^{N} d_i^2} \pm \sqrt{\frac{1}{N-1}\sum_{i=1}^{N}(d_i - d_S)^2}$, with d_i the i-th particle size and N the total number of measured particles. Only the relevant part of the log-normal distribution (>1% of maximum) was considered for the calculation of the average particle sizes.

Powder X-ray diffractograms were recorded on a Bruker AXS D2 Phaser diffractometer at room temperature with a fixed divergence slit. Samples were irradiated by Co Kα radiation (λ = 1.790 Å) at 30 kV and 10 mA. Not only fresh catalysts, but also used catalysts were analyzed. These were exposed to ambient conditions, separated from the SiC in the reactors, finely ground, and characterized without any further pretreatment.

Temperature-programmed reduction (TPR) profiles were obtained on a Micromeritics AutoChem II 2920 apparatus. The sample (50 mg, <75 μm granulites) was first dried *in situ* under an Ar flow at 1 L min^{-1} g_{sam}^{-1} at 393 K for 30 min. The cooled sample was then exposed to 5 vol % H_2/Ar at the same flow and heated to 873 K with a ramp of 2 K min^{-1}. The formed H_2O was captured with a dry ice/isopropanol cold trap, and the reduction profiles were recorded with a thermal conductivity detector (TCD). The H_2 reduction profiles of the CuZn-15/C and CuZn-15/SiO_2 catalysts (25−75 μm) were also obtained at a temperature ramp of 5 K min^{-1} in a 0.5 L min^{-1} g_{sam}^{-1} flow without prior drying to directly compare with the H_2 treatment during XAS.

Time-resolved, *operando* X-ray absorption spectroscopy (XAS) measurements on simultaneously the Cu (8979 eV) and Zn K-edges (9659 eV) were performed at the SOLEIL synchrotron (ROCK beamline).[52] Typically, *ca.* 3.5 mg of catalyst (25−75 μm sieve fraction) was loaded in a quartz capillary (ID 1.5 mm, 50 μm thick), which was tightly glued into a frame connected to gas feed lines. Heating of the capillary was ensured by a hot gas blower (FMD Oxford). After the capillary was leak-checked at 20 bar, XAS data was obtained in He at room temperature. The catalyst was exposed to a 15 mL min^{-1} flow of 20 vol % H_2/He and heated to 543 K (ramp 5 K min^{-1}) with a hold time of 5−15 min at ambient pressure. After the H_2 treatment, the capillary was cooled to 453 K prior to introducing a syngas feed (H_2/CO/He = 60/30/10 vol %) at 15 mL min^{-1}. Within *ca.* 100 min, the capillary was pressurized to 20 bar, and subsequently, the temperature was increased to 533 K (ramp 5 K min^{-1}) and held for 160 min. Only for the CuZn-15/C catalyst was the feed subsequently switched to H_2/CO/CO_2/He = 60/27/3/10 vol %, recording XAS spectra for 160 min, and after that to H_2/CO_2/He = 67.5/22.5/10 vol %. Finally, XAS data were recorded after cooling to room temperature at 20 bar and in the last experienced gas atmosphere (H_2/CO_2/He and H_2/CO/He for the CuZn-15/SiO_2 and CuZn-15/C catalysts, respectively).

During all treatments, XAS spectra were recorded while scanning the X-ray energy from 8.70 to 10.65 keV (20 averaged scans per 10 s) in transmission mode using a Si(111) quick-XAS monochromator. Methanol production and gas compositions were recorded with a mass spectrometer (Cirrus, MKS) at ambient pressure. If the measurement involved CO, a conditioned carbonyl trap was used upstream the capillary to capture metal carbonyl compounds. ZnO (abcr, 99.999%), CuO (Sigma-Aldrich, 99.999%), Cu_2O (Sigma-Aldrich, ≥99.99%), in-house synthesized Zn_2SiO_4 (Figure S27), all mixed with boron nitride (Sigma-Aldrich, 98%), and Cu (6 μm) and Zn (5 μm) foils were used as references, with their spectra being recorded at room temperature under air. A $Zn_{30}Cu_{70}$ brass measured at the ESRF (LISA beamline (BM 08)) was also used as a reference. The optics and performance at the two beamlines are different, and hence, this might give rise to slight changes in the observed XAS spectra. Data analysis was performed using Athena and Artemis software, as further detailed in supplementary section S4.

2.3. Catalyst Testing. A 16-reactor setup (Flowrence, Avantium) was used to evaluate the catalyst performance for methanol synthesis at 40 bar(g) and 533 K for at least 100 h. The powdered catalysts were pressed, crushed, and sieved into granules of 75−150 μm and were loaded (3−180 mg) in the stainless-steel reactors (ID 2.6 mm). The catalysts were diluted with SiC (212−245 μm fraction, Alfa Aesar, ≥98.8%, 46 grit), resulting in SiC contents between 22 and 88 vol % of the total packed catalyst bed.[53] The SiC had been previously calcined at 1073 K for 10 h, washed with 65 wt % HNO_3, rinsed with Milli-Q water until pH 7 was reached, and dried in static air at 393 K overnight. The varying catalyst loadings enabled us to achieve similar CO (+ CO_2) conversions (*ca.* 10%). The difference in sieve fractions between the catalysts and diluent facilitated postanalysis by EM and XRD.

An *in situ* reduction was performed in 2.8 mL min^{-1} of 5 vol % H_2/N_2 at 523 K for 3 h after which the temperature was lowered to 393 K. The reactors were exposed to a 2.2 mL min^{-1} flow of CO_2-free syngas (H_2/CO/He = 60/30/10 vol %) or CO_2-enriched syngas (H_2/CO/CO_2/He = 60/27/3/10 vol %), leading to a flow of 0.2−2.1 L min^{-1} g_{Cu}^{-1} and a gas-hourly space velocity (GHSV) of 400−53 200 h^{-1}. The reactors were pressurized to 40 bar(g), heated to 533 K (ramp 2 K min^{-1}), and the reaction was run for at least 100 h. Alternatively, the ZnO_x/C and ZnO_x/SiO_2 catalysts were alternately exposed to the predefined H_2/CO/He and H_2/CO/CO_2/He feeds. A triphase carbonyl trap (activated carbon, γ-Al_2O_3, ZnO) was located upstream of the CO feed to remove metal carbonyls and sulfur species. Products were periodically analyzed by online gas chromatography every 15 min. After catalysis, the samples were slowly exposed to air at 393 K. Details on the calculations of activity, selectivity, and stability are given in section S5.

3. RESULTS AND DISCUSSION

3.1. Structural Properties of the Catalysts. Figure 1 shows representative electron micrographs, including elemental maps, of CuZn-15/SiO_2 (frames A−C) and CuZn-15/C (frames D−F) catalysts both with 8.1 wt % Cu and 1.8 wt % ZnO (see Figures S2−S5 for other catalysts and zoomed-out micrographs). Note that the number in the catalyst names refers to the Zn/(Cu + Zn) fraction of 15 at%. The silica as support consists of aggregated spheres of *ca.* 8 nm, whereas the graphitic carbon has a sheet-like morphology of a few nanometers thick. Both materials have a high specific surface area (>260 m^2 g^{-1}), and *ca.* 50−60% of the total pore volume consists of mesopores (Figure S1, Table S1), making these materials suitable supports for model catalyst studies.Frame A shows no clear Cu(Zn)O_x nanoparticles on the silica support, demonstrating that it was challenging to distinguish metal particles on the silica support because of the limited phase contrast. Only by imaging ultramicrotomed slices were we able to obtain a representative HAADF-STEM micrograph with an elemental map (frame B). Cu(Zn)O_x particles of *ca.* 3−4 nm (bright spots) were observed for the CuZn-15/SiO_2 catalyst, corresponding to mainly Cu species (blue dots) and ZnO_x species (red dots). The distribution of Cu and ZnO_x looked similar after 150 h of catalysis (frame C), which is probably more representative for the catalyst during catalysis.

https://doi.org/10.1021/acscatal.1c05101
ACS Catal. 2022, 12, 6628−6639

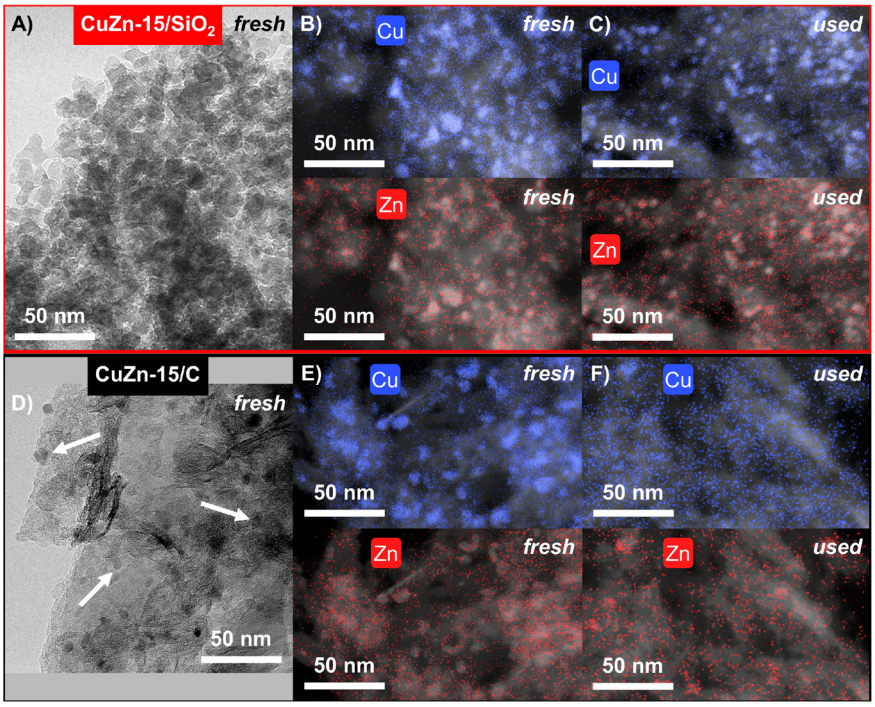

Figure 1. Representative EM images of the (A–C) CuZn-15/SiO_2 and (D–F) CuZn-15/C catalysts. Frames A and D involve BF-TEM, and frames B–C and E–F involve HAADF-STEM with an elemental map overlay. Number-averaged Cu(Zn)O_x particle sizes are 3.4 ± 0.8 nm (frames B–C) and 4.2 ± 1.7 nm (frame D) for the fresh CuZn-15/SiO_2 and CuZn-15/C catalysts, respectively. The used catalysts (frames C and F) are after 150 and 100 h of catalysis in an H_2/CO/CO_2 feed, respectively. Please note that the pixel size in frame F is larger (521 pm) than in frames B, C, and E (368 pm). Corresponding zoomed-out images and EDX spectra are shown in Figures S5–S6.

When using a graphitic support (frame D) CuO_x nanoparticles of *ca.* 4 nm were clearly discernible by TEM and well-distributed (dark spots indicated with white arrows) on the carbon surface (light gray).

The distribution was confirmed by the elemental maps of Cu and Zn species, projected on a HAADF-STEM image (frame E). There was a strong correlation between the location of the Cu nanoparticles and the distribution of the ZnO_x species, both in the fresh CuZn-15/C catalyst and after catalysis (frames E and F). The characteristics of the full series carbon-supported $CuZnO_x$/C catalysts both in the fresh and used state can be found in the Supporting Information (Table S2) and shows similar Cu(Zn)O_x particle sizes (d_N = 5–9 nm) with varying ZnO_x loadings. Additional structural information includes N_2 physisorption (Figure S1), additional electron microscopy imaging (Figures S2–S5), X-ray diffraction (XRD) analysis (Figure S8), and H_2 reduction profiling (Figure S9). Overall, we showed that in both catalysts well-distributed Cu(Zn)O_x particles of similar size were present and that the relatively thin sheets of graphitic carbon as a model support facilitated the determination of the particle sizes by electron microscopy.

3.2. Influence of the Support and Feed Composition.

In this section, we compare the catalytic performance of CuZn-15/SiO_2 and CuZn-15/C catalysts, which were prepared and tested in the same way and have similar Cu(Zn)O_x particle sizes and ZnO_x loadings but only have a different support. Figure 2 shows the methanol formation rate under industrially relevant temperature and pressure as a function of time in an H_2/CO feed as well as in an H_2/CO/CO_2 feed (mimicking industrially relevant conditions[1−5]). Figure S10 gives the CO (+ CO_2) conversion and total activity, and Table S4 provides additional information on the conversion levels, turnover frequencies (TOFs), and Cu(Zn)O_x particle growth during catalysis.

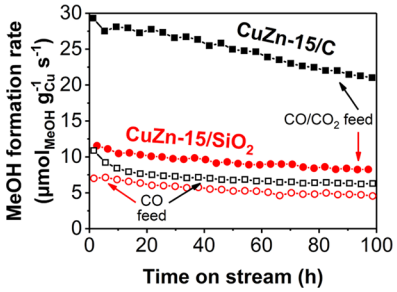

Figure 2. Methanol formation rate of the CuZn-15/SiO_2 (red circles) and CuZn-15/C (black squares) catalysts in a CO_2-free (open symbols) or -enriched (filled symbols) syngas feed. The data points of the CuZn-15/C catalyst in H_2/CO and H_2/CO/CO_2 are the average over 4 and 2 separate runs, respectively. Conditions: 533 K, 40 bar(g), H_2/CO/He = 60/30/10 vol % or H_2/CO/CO_2/He = 60/27/3/10 vol %.

The TOF for the carbon-supported catalyst ($3.9–15.3 \times 10^{-3}$ s^{-1}) was always higher than for the silica-supported catalyst ($1.6–3.0 \times 10^{-3}$ s^{-1}) (Table S4). Strikingly, the beneficial effect of CO_2 enrichment of the syngas feed on the methanol formation rate was much larger for the CuZn-15/C catalyst (factor 3.5) than for the CuZn-15/SiO_2 catalyst (factor 1.7) (Figure 2). Upon CO_2 enrichment the methanol selectivity increased from 83 to 99%$_C$ and from 85 to 98%$_C$ after 100 h on stream for, respectively, the CuZn-15/SiO_2 and CuZn-15/C catalysts, in line with earlier published results[5] and significantly higher than recently reported for $CuZnO_x/Al_2O_3$.[24] In the literature, enhancement factors upon CO_2 enrichment of 2–4

https://doi.org/10.1021/acscatal.1c05101
ACS Catal. 2022, 12, 6628−6639

are reported for $Cu/ZnO/Al_2O_3$ catalysts depending on the reaction conditions,[2,3,47] and differences were also observed between silica- and alumina-supported $CuZnO_x$ particles.[24] However, our results, obtained in the same reaction conditions and with similar Cu particles sizes, unequivocally proves that promotion with a given amount of ZnO_x is much more efficient using a carbon than using an oxide support. Under all conditions, the ZnO_x promotion is more effective in the CuZn-15/C catalyst than in the $CuZn-15/SiO_2$ catalyst, but the effect is especially pronounced with CO_2 enrichment of the feed.

It is known that ZnO_x itself can also act as a methanol synthesis catalyst, albeit with a lower activity than in combination with Cu.[16,54,55] Supported ZnO_x species without Cu were investigated under similar reaction conditions to check if the catalysis by ZnO_x on graphitic carbon contributed significantly. The ZnO_x/SiO_2 and ZnO_x/C catalysts have the same ZnO loading (both 10 wt %) with ZnO_x particle sizes of 7.7 and *ca.* 4.5 nm, respectively. Figure 3 shows the CO (+ CO_2) conversion versus time on stream in the presence and absence of CO_2 and for both an oxidic and a carbon support.

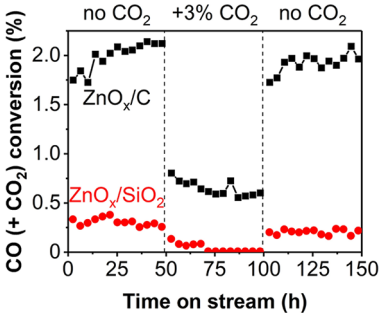

Figure 3. CO (+ CO_2) conversion of silica- and carbon-supported ZnO_x (10 wt %) in various syngas compositions. Label "+3% CO_2" in the total feed corresponds to a $CO_2/(CO + CO_2)$ volume fraction of 0.10. Conditions: 533 K, 40 bar(g), $H_2/(CO + CO_2)/He$ = 60/30/10 vol %, 21.9 mL min^{-1} g_{cat}^{-1}.

Irrespective of the syngas composition, carbon-supported ZnO_x species were much more active than silica-supported ZnO_x species, even when taking the slightly different Zn surface areas into account (Figure S12). EM analysis showed no Zn-based nanoparticles (Figure S4) in the fresh ZnO_x/SiO_2 catalyst (frame B), whereas they were present in the ZnO_x/C catalyst (frame A). During pure CO hydrogenation, the ZnO_x/C catalyst had a significant conversion of *ca.* 2% (of which *ca.* 1.3% was methanol (Figure S12)). The activity of both supported ZnO_x species clearly decreased in the presence of CO_2. The conversion level was restored when switching back to an H_2/CO feed. This demonstrates that the negative CO_2 effect on the conversion is not related to, for example, irreversible changes in the catalyst morphology but probably can be attributed to the significant reduction of ZnO in a CO_2-free feed, making it a more efficient methanol synthesis catalyst. Yet, the activity of the supported ZnO_x was too small to explain the overall effects of CO_2-enrichment in methanol synthesis of $CuZnO_x$-based catalysts. Nevertheless, these results clearly show that an oxide support has a strong interaction with the ZnO_x and leads to a different speciation than for the weaker interacting carbon supports.

3.3. Influence of the ZnO_x Loading on Activity and Stability. For the carbon-supported catalysts, we investigated in more detail the effect of the ZnO_x loading on the activity and stability of supported Cu nanoparticles. Figure 4 shows the

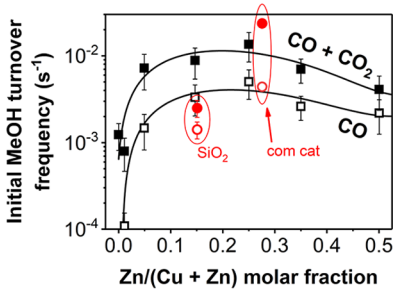

Figure 4. Initial methanol turnover frequency (TOF_{MeOH}) of $CuZnO_x/C$ (black squares) and metal oxide-supported (red circles) catalysts in an H_2/CO (open symbols) or an $H_2/CO/CO_2$ (filled symbols) feed (at t = 0). "SiO_2" = $CuZn-15/SiO_2$ catalyst. "com cat" = commercial, coprecipitated $Cu/ZnO/Al_2O_3/MgO$ catalyst (58 wt % Cu, *ca.* 10 nm CuO particles). Conditions: 533 K, 40 bar(g), $H_2/CO/He$ = 60/30/10 vol % or $H_2/CO/CO_2/He$ = 60/23/7/10 vol %.

specific activity (see Figures S13−S14 for the total activity) as a function of the ZnO_x loading in a syngas atmosphere with and without CO_2 (please note the logarithmic scale) for *ca.* 5.1 nm Cu nanoparticles supported on either a carbon support (black lines) or an oxide support (red markers). The activity increased when CO_2 was in the feed for all studied ZnO_x-promoted catalysts. After the initiation period, all catalysts had a methanol selectivity of >97%$_C$ in CO_2-enriched syngas. The highest TOF_{MeOH} values were obtained for carbon-supported catalysts with Zn/(Cu + Zn) molar fractions between 0.15 and 0.25, irrespective of the presence of CO_2 in the feed. These ZnO_x loadings are lower than the well-established optimal loading for the commercially used $Cu/ZnO/Al_2O_3/MgO$ methanol synthesis catalyst as well as for other oxide-based Cu catalysts in literature (Zn/(Cu + Zn) content of 29−47 at %).[10,13,15,19,22,23,28−31,56]

Another important factor in catalysis is the stability. In Figure S15, this stability is defined as the ratio between the activity after 100 h and after 50 h on stream. The addition of only 5 at% ZnO_x was sufficient to increase the catalyst stability from 74 ± 8% to 84 ± 3% upon syngas conversion. Further increasing the ZnO_x content to 15−35 at% maximized the stability to 91 ± 2% and 83 ± 3% in an H_2/CO and $H_2/CO/CO_2$ feed, respectively. In the most heavily promoted CuZn-50/C catalyst, the stability was somewhat lower. The presence of 15−35 at% ZnO_x apparently limited the $CuZnO_x$ particle growth during catalysis as evident from TEM and XRD analysis (Figures S3, S7, and S8) and is in line with the stability improvement for intermediate amounts of ZnO_x. Hence, ZnO_x is not only an activity promoter but also a stability promoter for carbon-supported Cu catalysts.

3.4. Catalyst Evolution during Reduction in H_2. From the literature, it is known that the coverage of the Cu surface with ZnO_x species[13] and the reduction degree of these ZnO_x species[14,35] are parameters that determine the effectiveness of ZnO_x as a promoter. However, mostly metal oxides are employed to support $CuZnO_x$ particles, which can result in the formation of spectator species such as zinc silicates and aluminates,[11,37,43] hampering the study of the active fraction of the ZnO_x promoter. The presence of the mixed Zn metal oxides may hence obscure the results also of, for example, electron energy loss spectroscopy (EELS) and *operando* X-ray absorption spectroscopy (XAS) measurements. While EELS is a valuable technique to study the local oxidation state of metals,[56,57] we chose to assess the chemical state of our supported catalysts by XAS because of the small particle sizes and relatively low metal

https://doi.org/10.1021/acscatal.1c05101
ACS Catal. 2022, 12, 6628−6639

loadings. Hence, our hypothesis was that our use of a carbon support would allow us to much better study the formation, oxidation state, and structure of the relevant ZnO_x promoter by time-resolved, *operando* XAS at simultaneously the Cu and Zn K-edges at 20 bar and up to 533 K.

A first piece of information about the interaction between CuO_x and ZnO_x species can be derived from the reduction profiles. Figure 5 shows the *ex situ* H_2 reduction profiles of the

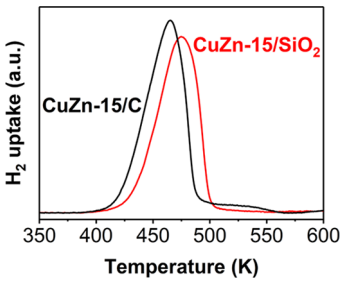

Figure 5. *Ex situ* reduction in 0.5 L min^{-1} g_{cat}^{-1} flow of 5 vol % H_2/Ar at 5 K min^{-1} in 1 bar, mimicking the conditions used during *in situ* H_2 treatment monitored by XAS.

$CuZn\text{-}15/SiO_2$ and CuZn-15/C catalysts. The theoretically maximum Cu surface coverage by a monolayer of Zn atoms is 75−95% for these catalysts with 15 at% ZnO_x. The maximum CuO reduction temperature (T_{max}) as well as the offset temperature for reduction (T_{offset}) were clearly lower for the CuZn-15/C catalyst than for the $CuZn\text{-}15/SiO_2$ catalyst (T_{max} of 465 *vs* 475 K, T_{offset} of 421 *vs* 434 K, respectively). Hence, the CuO is more easily reduced on a carbon support than on a silica support. We ascribe this to a stronger interaction of CuO_x with silica.

The reducibility of the $CuZn\text{-}15/SiO_2$ and CuZn-15/C catalysts was also investigated with *in situ* XAS under similar conditions as for the *ex situ* H_2 treatments. Time-resolved X-ray absorption spectra (Figure S16) were analyzed by fitting linear combinations of the macrocrystalline references to extract the Cu oxidation state evolutions (Figure S17), showing that the CuO species in both catalysts were fully reduced to Cu^0 *via* the formation of Cu^+ upon an H_2 treatment up to 543 K for 5−15 min. This was confirmed by a more in-depth study using multivariate analysis in which no prior information on the component spectra was imposed but which yielded eigenspectra that corresponded well to the macrocrystalline Cu references (Figure S18). This full reduction of CuO in ZnO_x-promoted CuO nanoparticles has also been reported in the literature.[14,24,42,58]

During the H_2 treatment we also studied changes in the ZnO_x oxidation state by *in situ* XAS. Figure 6 presents the time-resolved, normalized X-ray absorption near edge structures (XANES) and first derivatives at the Zn K-edge before and upon the H_2 treatment. We start with ZnO_x species in the Zn(II) oxidation state for both $CuZn\text{-}15/SiO_2$ (frames A and C) and CuZn-15/C (frames B and D) catalysts, as clear from the comparison to the first derivative of the ZnO reference. Upon heating in an H_2 atmosphere the Zn K-edge shifted to a lower energy (indicated by the arrows), showing that partially reduced ZnO_x was formed in both catalysts. The dominant features were still due to the presence of Zn^{2+}, as clear from the peak at 9.6626 keV on the first derivatives, although its intensity had slightly decreased.

Interestingly, the $CuZn\text{-}15/SiO_2$ catalyst (frame A) displayed two distinct peaks in the normalized XANES spectra (indicated with α and β). This peak combination has been reported before and is ascribed to the presence of zinc silicates in a single phase such as Zn_2SiO_4.[37,59−62] Yet, the CuZn-15/C catalyst (frame B)

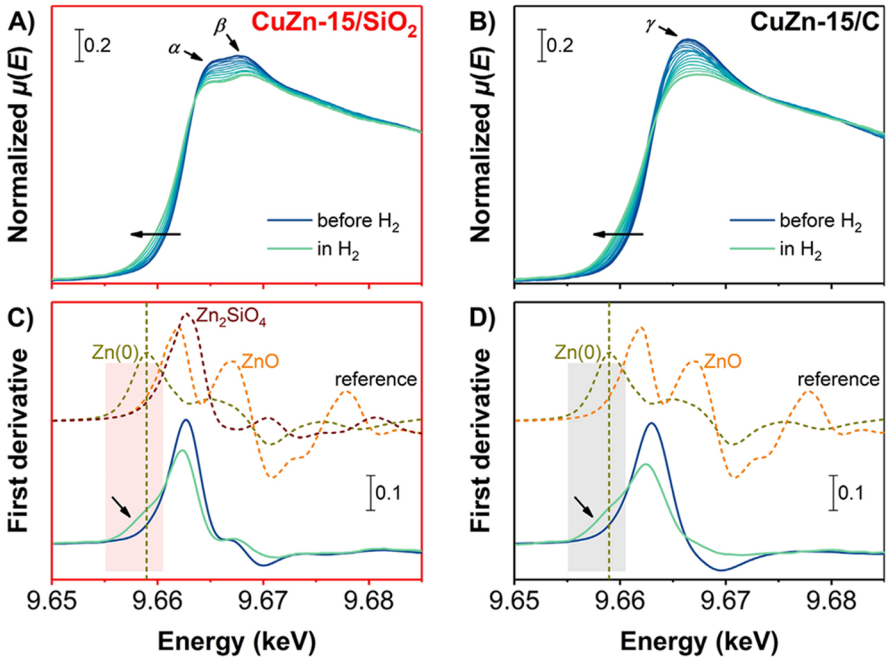

Figure 6. (A,B) Time-resolved, normalized absorption and (C,D) corresponding first derivatives of *in situ* XANES spectra at the Zn K-edge of the (A,C) $CuZn\text{-}15/SiO_2$ and (B,D) CuZn-15/C catalysts (solid lines). The spectra are depicted in the initial state at 298 K, during a treatment in 20 vol % H_2/He up to 543 K in 1 bar each *ca.* 5.7 min, and finally in an H_2 atmosphere at 453 K. Dashed lines show the first derivatives of macrocrystalline ZnO, Zn_2SiO_4, and Zn foil references at 298 K.

https://doi.org/10.1021/acscatal.1c05101
ACS Catal. 2022, 12, 6628−6639

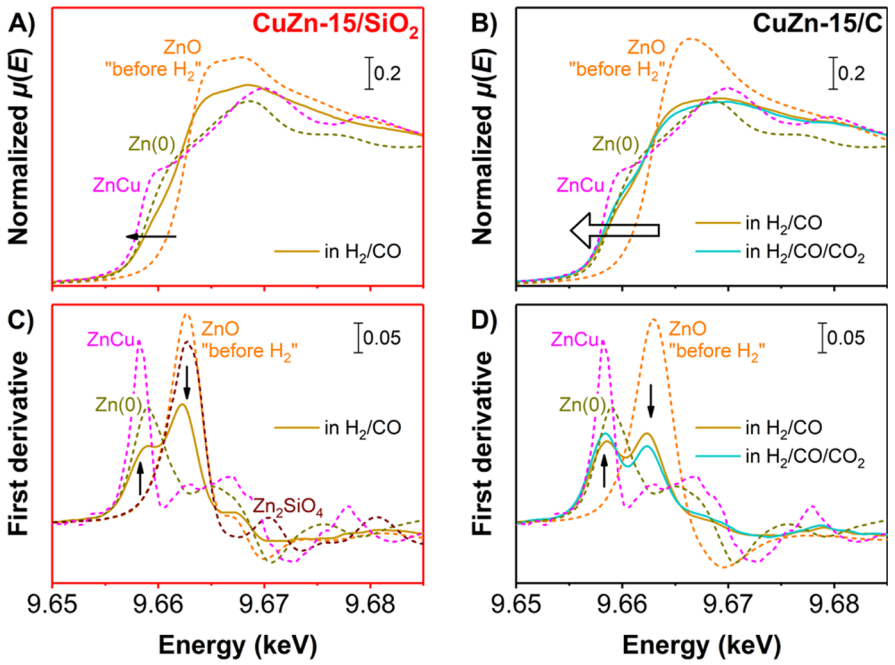

Figure 7. (A,B) Normalized absorption and (C,D) corresponding first derivatives of *operando*, normalized XANES spectra at the Zn K-edge of the (A,C) CuZn-15/SiO_2 and (B,D) CuZn-15/C catalysts (solid lines). Depicted during H_2/CO (and subsequent H_2/CO/CO_2) conversion at 20 bar and 533 K, each after 160 min. Gas compositions: H_2/CO/He = 60/30/10 vol % and H_2/CO/CO_2/He = 60/27/3/10 vol %. Dashed lines show the initial catalyst state (ZnO), macrocrystalline Zn_2SiO_4 and $Zn_{30}Cu_{70}$, and Zn foil at 298 K.

only had one single, broad peak (indicated with γ), in line with a ZnO_x phase which was also observed in electron microscopy (Figure 1, frame E). The estimated, average Zn oxidation number (ON) was slightly lower for the CuZn-15/C catalyst than for the CuZn-15/SiO_2 catalyst (+1.3 *vs* +1.6, see also Table S5). Multivariate analysis on the Zn K-edge is more challenging than for the Cu K-edge, as the XAS signal is lower. Extraction of the components (Figure S20) suggests the presence of three distinct phases for the CuZn-15/SiO_2 catalyst. The eigenspectrum of one of the components resembles that of Zn_2SiO_4 and its contribution is relatively stable throughout the experiment, indicating the presence of a substantial amount of Zn spectator species in the CuZn-15/SiO_2 catalyst. It has to be noted that because of the relatively low Zn loading, these spectator species were not observed by infrared spectroscopy (Figure S26). For the carbon-supported catalyst, a significant contribution of a compound with a relatively high absorption at lower energies is found (Figure S20). The phases do not fully match with the macrocrystalline Zn references, which indicates highly dispersed species of low crystallinity and/or not very well-defined mixed phases. This confirms the impact of the support on the ZnO_x speciation: on an oxidic support, the majority of the Zn species is irreducibly bound to the oxidic support and a fraction of the Zn is bound in silicate species, while on a carbon support a highly dispersed ZnO_x phase with an average Zn oxidation number significantly lower than +2 is present, which might be due to a high defect density in the ZnO (creating oxygen vacancies and a lower average ZnO state) or possibly the intermixing of fully reduced Zn in the compounds.

3.5. Nature of the ZnO_x under Working Conditions. The *in situ* H_2-treated catalysts were used for high-pressure methanol synthesis by CO, CO/CO_2, and CO_2 hydrogenation. Upon catalysis, no significant changes in the oxidation state and local coordination of the Cu^0 were detected (Figure S21), in line with results published earlier.[39,45] Figure 7 shows the normalized, *operando* XAS spectra of the Zn K-edge in the XANES region after 160 min in an H_2/CO feed and after 160 min of subsequent H_2/CO/CO_2 feed for the CuZn-15/SiO_2 (frames A and C) and CuZn-15/C (frames B and D) catalysts. The overall results, including CO_2 hydrogenation, are shown in Figures S19 and S21−S24. Note that because of the XAS setup restrictions, the amount of catalyst and hence the conversion was limited (Figure S25). For the CuZn-15/SiO_2 catalyst, the ZnO_x was only slightly further reduced during methanol synthesis (frames A and C) with an estimated Zn ON of +1.1. This was confirmed by a measurement after cooling the catalyst down to room temperature to obtain sharper features (average Zn ON of +1.2, Figure S19). Features that were attributed to zinc silicates were dominant at all stages in the XAS spectra for the CuZn-15/SiO_2 catalyst, as confirmed by multivariate analysis (Figure S20). The fact that only a slight reduction of the Zn(II) is observed when using oxidic supports and that the Zn species strongly interact with the support is in line with earlier reports using oxidic supports.[37,45]

Remarkably, in the CuZn-15/C catalyst, a large fraction of metallic Zn was formed during methanol synthesis at 20 bar (Figure 7, frames B and D). This observation was confirmed by multivariate analysis, which showed a resemblance of the independently extracted eigenspectrum of the Zn species to the XAS spectrum of metallic Zn (Figure S20). The average Zn ON was only *ca.* + 0.6. Assuming that the Zn species are either in the Zn(II) or Zn(0) oxidation state, this means that about 70% of the Zn species was completely reduced. With the addition of 3 vol % CO_2 in the feed, a slightly less-reducing gas atmosphere was created. Nevertheless, the Zn ON decreased further with time to *ca.* + 0.5 after nearly 3 h in the H_2/CO/CO_2 feed, which is probably rather an effect of time than feed composition. Upon switching to a pure H_2/CO_2 feed, the average Zn ON slightly increased to + (0.6−0.8). An increase is expected in a more oxidizing gas feed, as it is also predicted computationally that

https://doi.org/10.1021/acscatal.1c05101
ACS Catal. 2022, 12, 6628−6639

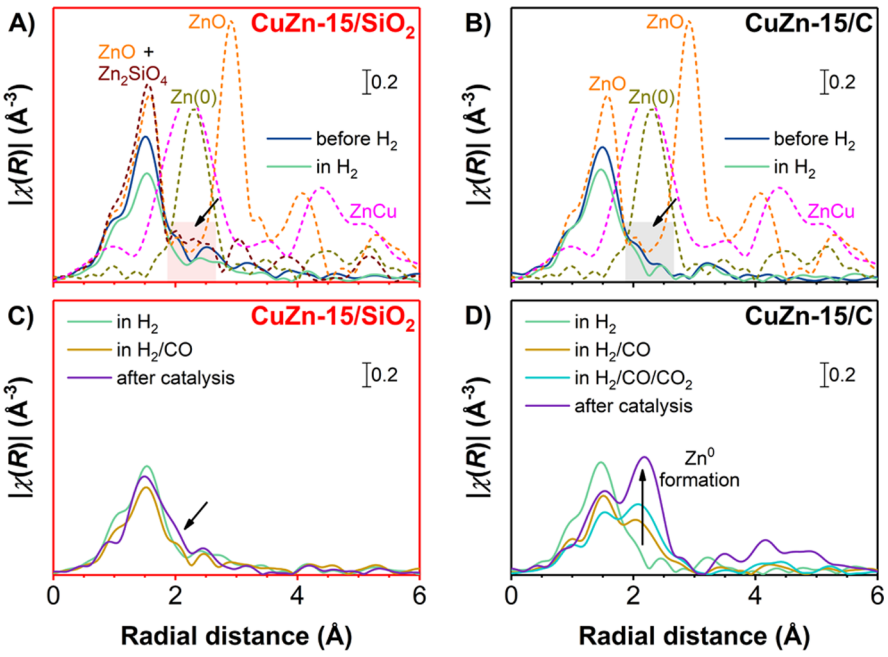

Figure 8. Fourier-transformed EXAFS spectra at the Zn K-edge of the (A,C) CuZn-15/SiO_2 and (B,D) CuZn-15/C catalysts (solid lines). (A,B) Depicted during *in situ* reduction in the initial state at 298 K and in an H_2 atmosphere at 453 K after an H_2 treatment at 1 bar (for conditions, see Figure 6). (C,D) Depicted during H_2/CO (and subsequent H_2/CO/CO_2) conversion at 533 K and 20 bar (for conditions, see Figure 7) and after catalysis. Dashed lines depict the macrocrystalline ZnO, Zn_2SiO_4, $Zn_{30}Cu_{70}$, and Zn foil references. The unlabeled arrows indicate the position of Zn−Zn or Zn−Cu bond formation.

there will be a slight dependence of the ON (and hence probably the Zn coverage) on the exact feed composition.[13] However, even under these conditions, most of the Zn species remain in the fully reduced state under *operando* conditions. This means that the relatively high Zn ONs in methanol synthesis systems reported until now (in the presence of an oxidic support) can probably be explained by a strong promoter−support interaction, and hence, a large fraction of the Zn promoter species is being chemically bound to the oxidic support (and hence inactive). In contrast, our use of a weakly interacting carbon support allows us to assess an average Zn oxidation state and coordination number that are much more representative of the true nature of the active ZnO_x promoter phase during methanol synthesis.

Several hypotheses have been postulated for the ZnO_x speciation during Cu-catalyzed methanol synthesis. First, the beneficial effect of the ZnO_x promoter was ascribed to the so-called strong metal−support interaction (SMSI) with slightly reduced ZnO having a high affinity for the Cu^0 metal and partially covering the Cu nanoparticle surface.[35,63] Alternative explanations involve the influence of ZnO_x on the structure of the Cu nanoparticles. For instance, it was proposed that specific steps sites were exceptionally active sites on the Cu^0 surface and that these step sites were stabilized by Zn^0 atoms.[10,39,64] Metallic Cu and Zn are quite miscible; up to 33 at% Zn can dissolve in Cu (solid solution) at temperatures between 473 K and the melting point (>1175 K).[65] Some groups proposed that the active site was related to the decoration of Cu^0 nanoparticles with Zn^0 atoms and shallow diffusion of Zn^0 atoms into the Cu surface.[13,21,44] However, results from *ex situ* and low-pressure studies have limited value, as it is known that the catalytically active phase dynamically adjusts to the working conditions.[66] A recent high-pressure *operando* study, based on oxidic supports, concluded that a distorted ZnO_x layer was the majority phase under working conditions with at most 9% of the Zn being present as Zn^0 atoms.[24] Our experiments clearly show that, if a strong interaction of the Zn species with an oxide support is avoided, a much more truthful picture of the active fraction of the Zn promoter species under high-pressure methanol synthesis conditions is obtained, and that this fraction is clearly reduced to zerovalent Zn upon prolonged methanol synthesis conditions (Figure 7).

Zooming in on the local coordination of the Cu and Zn atoms during high-pressure methanol synthesis, we analyzed the extended X-ray absorption fine structure (EXAFS) region of the XAS data. Figure 8 shows the EXAFS data on the Zn K-edge in *R*-space for the CuZn-15/SiO_2 (frame A) and CuZn-15/C (frame B) catalysts in the initial state and upon heating in an H_2 atmosphere. The EXAFS-derived *R*-spaces at the Cu K-edge and the EXAFS fitting parameters are available in Figure S24 and Tables S6−S9, respectively. The initial spectra of both catalysts have a main peak at 1.50 Å in the Fourier transform, which corresponds to first-shell Zn−O bonds such as in ZnO with a bond length of 1.97 Å. The *R*-space of the CuZn-15/SiO_2 catalyst (frame A) closely resembles that of the Zn_2SiO_4 reference, showing that a majority of the Zn atoms is bound to the oxide support, as reported before.[37] No contribution of second-shell Zn−Zn bonds was observed (frames A and B) (which could be expected in crystalline ZnO at 2.91 Å in the nonphase corrected Fourier transform, corresponding to a real bond length of of 3.2 Å[41]), indicating the absence of larger ZnO crystallites in both samples and in line with the high ZnO_x dispersion observed by TEM (Figure 1). During *in situ* H_2 reduction, the Zn−O bond intensity at 1.50 Å apparently decreased for both catalysts, but this was simply due to the increasing measurement temperature[35] as the overall peak intensities significantly increased in the spectra taken at room temperature after catalysis (purple lines in frames C and D)

https://doi.org/10.1021/acscatal.1c05101
ACS Catal. 2022, 12, 6628−6639

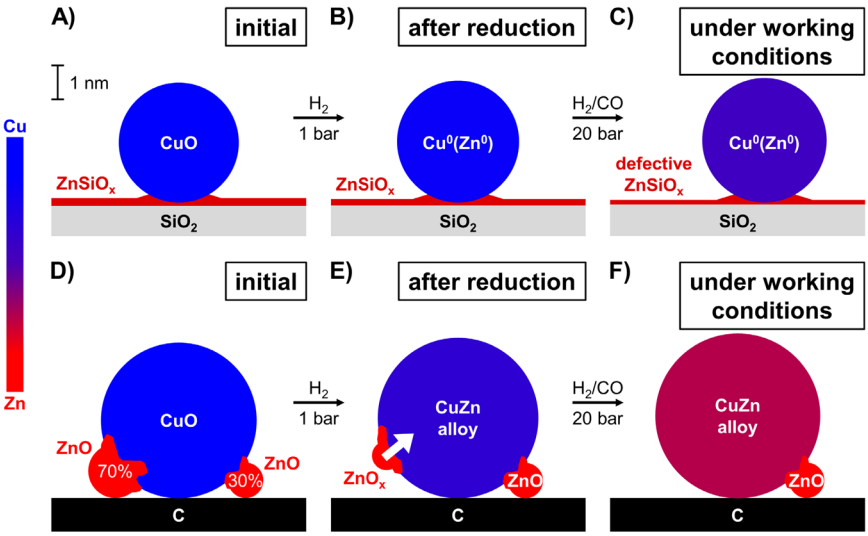

Figure 9. Schematic representation of the ZnO_x speciation in the (A-C) CuZn-15/SiO_2 and (D-F) CuZn-15/C catalysts, depicted (A,D) in the initial state, (B,E) after reduction, and (C,F) under working conditions at 20 bar and 533 K. The various shades of between blue (Cu) and red (Zn) in the CuZn particles represent the relative extent of Zn^0 incorporation into the Cu^0 nanoparticles based on the estimated Zn ONs from the XANES analysis. For frames B and C, separate Cu^0 nanoparticles may exist next to alloyed CuZn particles.

compared with the spectra taken during the last stage of catalysis at high temperature. It is important to note that in neither of the catalysts was Zn^0 formation observed during reduction in atmospheric-pressure H_2 (the Zn−Zn or Zn−Cu bond fingerprint is expected at 2.30 Å in the nonphase corrected Fourier transform, its position is indicated with an unlabeled arrow in the frames). After the *in situ* H_2 reduction, the first-shell Cu−Cu coordination number (CN) in metallic Cu was *ca.* 11 (for bulk Cu^0 this CN is 12), and it remained unchanged for both catalysts, independent of the exact feed. This means that no change in the Cu nanoparticles was observed upon exposure to working conditions: neither a significant fraction of oxidized copper nor the presence of highly dispersed copper. This is in agreement with the fully reduced Cu observed in the spectra at the XANES region.

We continue the EXAFS analysis under *operando* methanol synthesis conditions by focusing on the Zn local surrounding. Figure 8 (frames C,D) shows selected *R*-spaces from the EXAFS data on the Zn K-edge for both catalysts (for the complete set, please see Figure S23). For the CuZn-15/SiO_2 catalyst during CO hydrogenation, only a very minor fraction of metallic Zn was observed (signal around 2.30 Å indicated with the arrow in frame C), in line with earlier reports on oxide-supported catalysts.[24,35,63] Nevertheless, a change was observed, as the first-shell Zn−O CN decreased from 4 (as in bulk ZnO and Zn_2SiO_4) to 2.6 ± 0.5 and a very low second-shell Zn−Zn or Zn−Cu (from here onward denoted as Zn−M) CN of 2.2 ± 1.4 was obtained (for bulk Zn^0 this CN is 12). This indicates a very slight change in the average Zn surroundings, but because of the small changes and the very similar Zn−Zn and Zn−Cu bonding distances, it is not possible to analyze this in detail. Overall, the signal remains dominated by features that are attributed to Zn silicate species, and there is very little difference between the reduced fresh catalyst and that under working conditions.

Interestingly, the CuZn-15/C catalyst (frame D) displayed large changes when switching to working conditions, which was already expected from the zerovalent Zn as evidenced by the XANES analysis (Figure 7, frame B). An average Zn−M bond length of 2.54 Å (close to that of 2.66 Å of the Zn^0 foil reference) and a quite high Zn−M CN of 6.1 ± 1.3 were obtained. This is a clear supporting evidence for the large fraction of zerovalent Zn species in the active catalysts. Upon prolonged exposure (while slightly enriching the feed with CO_2), the increase in coordination number continues to a Zn^0 CN of *ca.* 8. This means that the majority of the Zn promoter species is present in metal nanoparticles. The very similar Zn−Zn and Zn−Cu bonding distances do not allow us to unequivocally derive the nature of these metal nanoparticles. However, the zerovalent Zn is very likely located in Cu−Zn nanoparticles. The high Zn−M coordination number suggests that the Zn does not remain as adatoms or a monolayer on the outside of the Cu particle. The diffusion coefficient of Zn^0 in Cu^0 strongly depends on the Cu particle size and temperature (see also Table S10)[67−69] but is high enough to support a full distribution of the Zn^0 throughout the relatively small Cu^0 particles at the time scale of hours, in line with the XRD pattern of the used CuZn-15/C catalyst showing a small downshift of the Cu^0 diffraction line and hence suggests CuZn alloy formation (Figure S8, frame D).

Interestingly, the time scale of the formation of highly coordinated zerovalent Zn is quite in line with the generally observed activation period for Cu methanol synthesis catalysts exposed to high-pressure working conditions.[5,9] To our knowledge, no clear explanation for this activation period has so far been reported in academic literature, but our results suggest that the gradual reduction of Zn(II) to active Zn(0) promoter species might be an important factor in this activation.

Figure 9 summarizes the results of our study by depicting the ZnO_x speciation in silica- and carbon-supported Cu catalysts containing 15 at% Zn/(Cu + Zn) after reduction as well as during high-pressure methanol synthesis. On both supports, the Cu^{2+} nanoparticles (depicted in dark blue) were fully reduced to Cu^0 nanoparticles in 5−15 min exposure to 1 bar H_2 at 543 K. Even during high-pressure methanol synthesis with a H_2/CO_2 feed, no significant subsequent change in the oxidation state of the Cu was observed. Using an oxidic support, which is standard in commercial catalysts and most academic studies, it was difficult to derive detailed information about the speciation of the Zn component (depicted in red) that was active as a

https://doi.org/10.1021/acscatal.1c05101
ACS Catal. 2022, 12, 6628−6639

promoter. Only slight changes in the average Zn speciation were observed (in line with earlier literature), as the signal was dominated by Zn species that had a strong interaction with the oxidic support (depicted as a layer of $ZnSiO_x$), and these species remained dominant under all (also methanol synthesis) conditions. In contrast, using a much less strongly interacting carbon support, allowed us to follow the fraction of the Zn species that was closely affiliated with the Cu nanoparticles and hence most likely represents the active Zn promoter species during catalysts. Under methanol synthesis conditions, the relevant ZnO_x phase is in a deeply reduced state with an average Zn oxidation number of only +0.6. Assuming that only Zn^{2+} and Zn^0 species exist, this means that *ca.* 70% of the ZnO is fully reduced to Zn^0. The Zn−M coordination number was as high as 8 during methanol synthesis working conditions, showing that the Zn^0 is almost fully coordinated with other metal atoms and has likely mostly diffused into the Cu nanoparticles. It is likely that this Zn speciation for the active promoter species is also relevant for the more conventional oxide-supported catalysts, to which much more Zn must be added to reach an optimum promoter effect, which is probably explained by the fact that a large fraction of the added Zn is not active as promoter.

4. CONCLUSIONS

Cu nanoparticulate catalysts on graphitic carbon were prepared, and compared to SiO_2-supported catalysts, to better understand the interaction between the Cu and the Zn-based promoter species and the speciation of Zn acting as a promoter during high pressure methanol synthesis. With a modest amount of ZnO_x promoter, the methanol formation for the $CuZnO_x/C$ catalyst was significantly faster than for a $CuZnO_x/SiO_2$ catalyst with similar Cu particle size in a pure H_2/CO feed. This difference was even much more pronounced in a CO_2-enriched syngas feed. Importantly, the use of graphitic carbon model supports allowed us to reveal the true speciation of the active fraction of the Zn-based promoter under commercially relevant methanol synthesis conditions. The vast majority of the Zn(II) is reduced all the way to Zn(0) during methanol synthesis at 20 bar. Also the Zn coordination number was high, making it likely that the Zn(0) diffused into the Cu nanoparticles. The characteristic time for this diffusion corresponds to the activation time that is generally observed with this type of catalysts. For the first time this gives direct insight into the nature of the active fraction of the Zn-based promoter in high pressure methanol synthesis, not obscured by the commonly large fraction of Zn species that strongly interacts with an oxidic support, and hence dominates the structural characterization results.

■ ASSOCIATED CONTENT

Supporting Information

The Supporting Information is available free of charge at https://pubs.acs.org/doi/10.1021/acscatal.1c05101.

Brief descriptions of electron imaging, crystallinity, reducibility, and the porosity of the catalysts; additional information on the catalyst activity and stability; complete set of XAS data; and details on the calculation of catalyst performance (PDF)

■ AUTHOR INFORMATION

Corresponding Author

Petra E. de Jongh − *Materials Chemistry and Catalysis, Debye Institute for Nanomaterials Science, Utrecht University, 3584 CG Utrecht, The Netherlands;* orcid.org/0000-0002-2216-2620; Email: P.E.deJongh@uu.nl

Authors

Remco Dalebout − *Materials Chemistry and Catalysis, Debye Institute for Nanomaterials Science, Utrecht University, 3584 CG Utrecht, The Netherlands*

Laura Barberis − *Materials Chemistry and Catalysis, Debye Institute for Nanomaterials Science, Utrecht University, 3584 CG Utrecht, The Netherlands*

Giorgio Totarella − *Materials Chemistry and Catalysis, Debye Institute for Nanomaterials Science, Utrecht University, 3584 CG Utrecht, The Netherlands*

Savannah J. Turner − *Materials Chemistry and Catalysis, Debye Institute for Nanomaterials Science, Utrecht University, 3584 CG Utrecht, The Netherlands*

Camille La Fontaine − *Synchrotron SOLEIL, L'Orme des Merisiers, Gif-sur-Yvette 91192 CEDEX, France*

Frank M. F. de Groot − *Materials Chemistry and Catalysis, Debye Institute for Nanomaterials Science, Utrecht University, 3584 CG Utrecht, The Netherlands;* orcid.org/0000-0002-1340-2186

Xavier Carrier − *Laboratoire de Réactivité de Surface, UMR CNRS 7197, Sorbonne Université, Paris 75252 CEDEX 05, France*

Ad M. J. van der Eerden − *Materials Chemistry and Catalysis, Debye Institute for Nanomaterials Science, Utrecht University, 3584 CG Utrecht, The Netherlands*

Florian Meirer − *Inorganic Chemistry and Catalysis, Debye Institute for Nanomaterials Science, Utrecht University, 3584 CG Utrecht, The Netherlands;* orcid.org/0000-0001-5581-5790

Complete contact information is available at: https://pubs.acs.org/10.1021/acscatal.1c05101

Author Contributions

R.D. and P.d.J. conceived and planned the experiments. R.D. measured the performance of the catalysts, analyzed the catalytic data, and drafted the manuscript together with P.d.J. S.T. performed electron microscopy imaging by EDX, and G.T. performed the ultramicrotomy. R.D., L.B., G.T., X.C., and P.d.J. performed the XAS experiments. C.L.F. designed the experimental method and assisted with data interpretation. L.B., G.T., A.v.d.E., F.M., and F.d.G. analyzed the XAS data. P.d.J. supervised the work. All authors contributed to the final manuscript.

Notes

The authors declare no competing financial interest.

■ ACKNOWLEDGMENTS

Lisette Pompe is thanked for the synthesis of several carbon-supported catalysts. We also thank Rolf Beerthuis and Jan Willem de Rijk for useful input during catalytic testing. We acknowledge SOLEIL for provision of synchrotron radiation facilities, and we would like to thank Valérie Briois for assistance in using the ROCK beamline and Laurent Barthe who helped with the installation of the setup (proposal ID 20190640). We thank Kai Han for providing the brass reference measured at the LISA beamline (BM 08) of the ESRF in Grenoble. Mahnaz Ghiasi Kabiri is thanked for discussion on the analysis of the XAS data. The work at ROCK was supported by a public grant overseen by the French National Research Agency (ANR) as

part of the *Investissements d'Avenir* program (reference: ANR10-EQPX45). This project has received funding from the European Research Council (ERC), ERC-2014-CoG, project number 648991.

REFERENCES

(1) Iaquaniello, G.; Cucchiella, B.; Antonetti, E. Method for Producing Synthesis Gas for Methanol Production. WO2013062413A1, 2013.
(2) Sahibzada, M.; Metcalfe, I. S.; Chadwick, D. Methanol Synthesis from $CO/CO_2/H_2$ over $Cu/ZnO/Al_2O_3$ at Differential and Finite Conversions. *J. Catal.* **1998**, *174* (2), 111−118.
(3) Lee, J. S.; Lee, K. H.; Lee, S. Y.; Kim, Y. G. A Comparative Study of Methanol Synthesis from CO_2/H_2 and CO/H_2 over a $Cu/ZnO/Al_2O_3$ Catalyst. *J. Catal.* **1993**, *144* (2), 414−424.
(4) Klier, K.; Chatikavanij, V.; Herman, R. G.; Simmons, G. W. Catalytic Synthesis of Methanol from CO/H_2: IV. The Effects of Carbon Dioxide. *J. Catal.* **1982**, *74* (2), 343−360.
(5) Dalebout, R.; Visser, N. L.; Pompe, C. E.; de Jong, K. P.; de Jongh, P. E. Interplay between Carbon Dioxide Enrichment and Zinc Oxide Promotion of Copper Catalysts in Methanol Synthesis. *J. Catal.* **2020**, *392*, 150−158.
(6) Nielsen, N. D.; Jensen, A. D.; Christensen, J. M. The Roles of CO and CO_2 in High Pressure Methanol Synthesis over Cu-Based Catalysts. *J. Catal.* **2021**, *393*, 324−334.
(7) Guil-López, R.; Mota, N.; Llorente, J.; Millán, E.; Pawelec, B.; García, R.; Fierro, J. L. G.; Navarro, R. M. Structure and Activity of Cu/ZnO Catalysts Co-Modified with Aluminium and Gallium for Methanol Synthesis. *Catal. Today* **2020**, *355*, 870−881.
(8) Zhang, F.; Liu, Y.; Xu, X.; Yang, P.; Miao, P.; Zhang, Y.; Sun, Q. Effect of Al-Containing Precursors on $Cu/ZnO/Al_2O_3$ Catalyst for Methanol Production. *Fuel Process. Technol.* **2018**, *178*, 148−155.
(9) Prieto, G.; de Jong, K. P.; de Jongh, P. E. Towards "greener" Catalyst Manufacture: Reduction of Wastewater from the Preparation of $Cu/ZnO/Al_2O_3$ Methanol Synthesis Catalysts. *Catal. Today* **2013**, *215*, 142−151.
(10) Behrens, M.; Studt, F.; Kasatkin, I.; Kühl, S.; Hävecker, M.; Abild-Pedersen, F.; Zander, S.; Girgsdies, F.; Kurr, P.; Kniep, B.-L.; Tovar, M.; Fischer, R. W.; Nørskov, J. K.; Schlögl, R. The Active Site of Methanol Synthesis over $Cu/ZnO/Al_2O_3$ Industrial Catalysts. *Science* **2012**, *336* (6083), 893−897.
(11) van den Berg, R.; Prieto, G.; Korpershoek, G.; van der Wal, L. I.; van Bunningen, A. J.; Lægsgaard-Jørgensen, S.; de Jongh, P. E.; de Jong, K. P. Structure Sensitivity of Cu and CuZn Catalysts Relevant to Industrial Methanol Synthesis. *Nat. Commun.* **2016**, *7*, 13057.
(12) Laudenschleger, D.; Ruland, H.; Muhler, M. Identifying the Nature of the Active Sites in Methanol Synthesis over $Cu/ZnO/Al_2O_3$ Catalysts. *Nat. Commun.* **2020**, *11*, 3898.
(13) Kuld, S.; Thorhauge, M.; Falsig, H.; Elkjær, C. F.; Helveg, S.; Chorkendorff, I.; Sehested, J. Quantifying the Promotion of Cu Catalysts by ZnO for Methanol Synthesis. *Science* **2016**, *352* (6288), 969−974.
(14) Frei, E.; Gaur, A.; Lichtenberg, H.; Zwiener, L.; Scherzer, M.; Girgsdies, F.; Lunkenbein, T.; Schlögl, R. Cu-Zn Alloy Formation as Unfavored State for Efficient Methanol Catalysts. *ChemCatChem.* **2020**, *12* (16), 4029−4033.
(15) Almusaiteer, K. A.; Al-Hadhrami, A.; Abed, O.; Biausque, G.; Al-Amer, A. Catalysts and Methods for Methanol Synthesis from Direct Hydrogenation of Syngas and/or Carbon Dioxide. US20190076828A1, 2019.
(16) Waugh, K. C. Methanol Synthesis. *Catal. Today* **1992**, *15* (1), 51−75.
(17) Chinchen, G. C.; Waugh, K. C.; Whan, D. A. The Activity and State of the Copper Surface in Methanol Synthesis Catalysts. *Appl. Catal.* **1986**, *25* (1−2), 101−107.
(18) Pan, W. X.; Cao, R.; Roberts, D. L.; Griffin, G. L. Methanol Synthesis Activity of Cu/ZnO Catalysts. *J. Catal.* **1988**, *114* (2), 440−446.
(19) Tisseraud, C.; Comminges, C.; Belin, T.; Ahouari, H.; Soualah, A.; Pouilloux, Y.; Le Valant, A. The Cu-ZnO Synergy in Methanol Synthesis from CO_2, Part 2: Origin of the Methanol and CO Selectivities Explained by Experimental Studies and a Sphere Contact Quantification Model in Randomly Packed Binary Mixtures on Cu-ZnO Coprecipitate Catalysts. *J. Catal.* **2015**, *330*, 533−544.
(20) Spencer, M. S. The Role of Zinc Oxide in Cu/ZnO Catalysts for Methanol Synthesis and the Water-Gas Shift Reaction. *Top. Catal.* **1999**, *8* (3−4), 259−266.
(21) Grunwaldt, J.-D.; Molenbroek, A. M.; Topsøe, N.-Y.; Topsøe, H.; Clausen, B. S. In Situ Investigations of Structural Changes in Cu/ZnO Catalysts. *J. Catal.* **2000**, *194* (2), 452−460.
(22) Kattel, S.; Ramírez, P. J.; Chen, J. G.; Rodriguez, J. A.; Liu, P. Active Sites for CO_2 Hydrogenation to Methanol on Cu/ZnO Catalysts. *Science* **2017**, *355* (6331), 1296−1299.
(23) Le Valant, A.; Comminges, C.; Tisseraud, C.; Canaff, C.; Pinard, L.; Pouilloux, Y. The Cu-ZnO Synergy in Methanol Synthesis from CO_2, Part 1: Origin of Active Site Explained by Experimental Studies and a Sphere Contact Quantification Model on Cu + ZnO Mechanical Mixtures. *J. Catal.* **2015**, *324*, 41−49.
(24) Divins, N. J.; Kordus, D.; Timoshenko, J.; Sinev, I.; Zegkinoglou, I.; Bergmann, A.; Chee, S. W.; Widrinna, S.; Karslıoğlu, O.; Mistry, H.; Lopez Luna, M.; Zhong, J. Q.; Hoffman, A. S.; Boubnov, A.; Boscoboinik, J. A.; Heggen, M.; Dunin-Borkowski, R. E.; Bare, S. R.; Roldan Cuenya, B. Operando High-Pressure Investigation of Size-Controlled CuZn Catalysts for the Methanol Synthesis Reaction. *Nat. Commun.* **2021**, *12*, 1435.
(25) Nakamura, J.; Fujitani, T.; Kuld, S.; Helveg, S.; Chorkendorff, I.; Sehested, J. Comment on "Active Sites for CO_2 Hydrogenation to Methanol on Cu/ZnO Catalysts. *Science* **2017**, *357* (6354), eaan8074.
(26) Nakamura, J.; Choi, Y.; Fujitani, T. On the Issue of the Active Site and the Role of ZnO in Cu/ZnO Methanol Synthesis Catalysts. *Top. Catal.* **2003**, *22* (3−4), 277−285.
(27) Behrens, M.; Zander, S.; Kurr, P.; Jacobsen, N.; Senker, J.; Koch, G.; Ressler, T.; Fischer, R. W.; Schlögl, R. Performance Improvement of Nanocatalysts by Promoter-Induced Defects in the Support Material: Methanol Synthesis over Cu/ZnO:Al. *J. Am. Chem. Soc.* **2013**, *135* (16), 6061−6068.
(28) Herman, R. G.; Klier, K.; Simmons, G. W.; Finn, B. P.; Bulko, J. B. Catalytic Synthesis of Methanol from CO/H_2 I. Phase Composition, Electronic Properties, and Activities of the $Cu/ZnO/M_2O_3$ Catalysts. *J. Catal.* **1979**, *56* (3), 407−429.
(29) Günter, M. M.; Ressler, T.; Bems, B.; Büscher, C.; Genger, T.; Hinrichsen, O.; Muhler, M.; Schlögl, R. Implication of the Microstructure of Binary Cu/ZnO Catalysts for Their Catalytic Activity in Methanol Synthesis. *Catal. Lett.* **2001**, *71* (1−2), 37−44.
(30) Fujitani, T.; Nakamura, J. The Effect of ZnO in Methanol Synthesis Catalysts on Cu Dispersion and the Specific Activity. *Catal. Lett.* **1998**, *56*, 119−124.
(31) Fujitani, T.; Nakamura, I.; Uchijima, T.; Nakamura, J. The Kinetics and Mechanism of Methanol Synthesis by Hydrogenation of CO_2 over a Zn-Deposited Cu(111) Surface. *Surf. Sci.* **1997**, *383* (2−3), 285−298.
(32) Kühl, S.; Tarasov, A.; Zander, S.; Kasatkin, I.; Behrens, M. Cu-Based Catalyst Resulting from a Cu,Zn,Al Hydrotalcite-like Compound: A Microstructural, Thermoanalytical, and in Situ XAS Study. *Chem. Eur. J.* **2014**, *20* (13), 3782−3792.
(33) Sun, Q.; Zhang, Y.-L.; Chen, H.-Y.; Deng, J.-F.; Wu, D.; Chen, S.-Y. A Novel Process for the Preparation of Cu/ZnO and $Cu/ZnO/Al_2O_3$ Ultrafine Catalyst: Structure, Surface Properties, and Activity for Methanol Synthesis from $CO_2 + H_2$. *J. Catal.* **1997**, *167* (1), 92−105.
(34) Clausen, B. S.; Lengeler, B.; Rasmussen, B. S. X-Ray Absorption Spectroscopy Study of Cu-Based Methanol Catalysts. 1. Calcined State. *J. Phys. Chem.* **1985**, *89* (11), 2319−2324.
(35) Großmann, D.; Klementiev, K.; Sinev, I.; Grünert, W. Surface Alloy or Metal-Cation Interaction-The State of Zn Promoting the Active Cu Sites in Methanol Synthesis Catalysts. *ChemCatChem.* **2017**, *9* (2), 365−372.

https://doi.org/10.1021/acscatal.1c05101
ACS Catal. 2022, 12, 6628−6639

(36) Großmann, D.; Dreier, A.; Lehmann, C.; Grünert, W. Methanol Synthesis over Cu-ZnO Aggregates Supported on Carbon Nanotubes. *Appl. Catal., A* **2015**, *504*, 351−360.
(37) Prieto, G.; Zečević, J.; Friedrich, H.; de Jong, K. P.; de Jongh, P. E. Towards Stable Catalysts by Controlling Collective Properties of Supported Metal Nanoparticles. *Nat. Mater.* **2013**, *12* (1), 34−39.
(38) Grandjean, D.; Pelipenko, V.; Batyrev, E. D.; van den Heuvel, J. C.; Khassin, A. A.; Yurieva, T. M.; Weckhuysen, B. M. Dynamic Cu/Zn Interaction in SiO_2 Supported Methanol Synthesis Catalysts Unraveled by in situ XAFS. *J. Phys. Chem. C* **2011**, *115* (41), 20175−20191.
(39) Naumann d'Alnoncourt, R.; Xia, X.; Strunk, J.; Löffler, E.; Hinrichsen, O.; Muhler, M. The Influence of Strongly Reducing Conditions on Strong Metal-Support Interactions in Cu/ZnO Catalysts Used for Methanol Synthesis. *Phys. Chem. Chem. Phys.* **2006**, *8* (13), 1525−1538.
(40) Frei, E.; Gaur, A.; Lichtenberg, H.; Heine, C.; Friedrich, M.; Greiner, M.; Lunkenbein, T.; Grunwaldt, J.-D.; Schlögl, R. Activating a Cu/ZnO:Al Catalyst - Much More than Reduction: Decomposition, Self-Doping and Polymorphism. *ChemCatChem.* **2019**, *11* (6), 1587−1592.
(41) Tohji, K.; Udagawa, Y.; Mizushima, T.; Ueno, A. The Structure of the Cu/ZnO Catalyst by an in-situ EXAFS Study. *J. Phys. Chem.* **1985**, *89* (26), 5671−5676.
(42) Kleymenov, E.; Sa, J.; Abu-Dahrieh, J.; Rooney, D.; van Bokhoven, J. A.; Troussard, E.; Szlachetko, J.; Safonova, O.; Nachtegaal, M. Structure of the Methanol Synthesis Catalyst Determined by in situ HERFD XAS and EXAFS. *Catal. Sci. Technol.* **2012**, *2* (2), 373−378.
(43) van den Berg, M. W. E.; Polarz, S.; Tkachenko, O. P.; Klementiev, K. V.; Bandyopadhyay, M.; Khodeir, L.; Gies, H.; Muhler, M.; Grünert, W. Cu/ZnO Aggregates in Siliceous Mesoporous Matrices: Development of a New Model Methanol Synthesis Catalyst. *J. Catal.* **2006**, *241* (2), 446−455.
(44) Zhang, Z.; Chen, X.; Kang, J.; Yu, Z.; Tian, J.; Gong, Z.; Jia, A.; You, R.; Qian, K.; He, S.; Teng, B.; Cui, Y.; Wang, Y.; Zhang, W.; Huang, W. The Active Sites of Cu-ZnO Catalysts for Water Gas Shift and CO Hydrogenation Reactions. *Nat. Commun.* **2021**, *12*, 4331.
(45) Zabilskiy, M.; Sushkevich, V. L.; Palagin, D.; Newton, M. A.; Krumeich, F.; Van Bokhoven, J. A. The Unique Interplay between Copper and Zinc during Catalytic Carbon Dioxide Hydrogenation to Methanol. *Nat. Commun.* **2020**, *11*, 2409.
(46) Zabilskiy, M.; Sushkevich, V. L.; Newton, M. A.; van Bokhoven, J. A. Copper-Zinc Alloy-Free Synthesis of Methanol from Carbon Dioxide over Cu/ZnO/Faujasite. *ACS Catal.* **2020**, *10*, 14240−14244.
(47) Robinson, W. R. A. M.; Mol, J. C. Support Effects in Methanol Synthesis over Copper-Containing Catalysts. *Appl. Catal.* **1991**, *76* (1), 117−129.
(48) Chatterjee, R.; Kuld, S.; van den Berg, R.; Chen, A.; Shen, W.; Christensen, J. M.; Jensen, A. D.; Sehested, J. Mapping Support Interaction in Copper Catalysts. *Top. Catal.* **2019**, *62* (7−11), 649−659.
(49) Schumann, J.; Eichelbaum, M.; Lunkenbein, T.; Thomas, N.; Álvarez Galván, M. C.; Schlögl, R.; Behrens, M. Promoting Strong Metal Support Interaction: Doping ZnO for Enhanced Activity of Cu/ZnO:M (M = Al, Ga, Mg) Catalysts. *ACS Catal.* **2015**, *5* (6), 3260−3270.
(50) Prieto, G.; Shakeri, M.; de Jong, K. P.; de Jongh, P. E. Quantitative Relationship between Support Porosity and the Stability of Pore-Confined Metal Nanoparticles Studied on $CuZnO/SiO_2$ Methanol Synthesis Catalysts. *ACS Nano* **2014**, *8* (3), 2522−2531.
(51) Thommes, M.; Kaneko, K.; Neimark, A. V.; Olivier, J. P.; Rodriguez-Reinoso, F.; Rouquerol, J.; Sing, K. S. W. Physisorption of Gases, with Special Reference to the Evaluation of Surface Area and Pore Size Distribution (IUPAC Technical Report). *Pure Appl. Chem.* **2015**, *87* (9−10), 1051−1069.
(52) La Fontaine, C.; Belin, S.; Barthe, L.; Roudenko, O.; Briois, V. ROCK: A Beamline Tailored for Catalysis and Energy-Related Materials from Ms Time Resolution to Mm Spatial Resolution. *Synchrotron Radiat. News* **2020**, *33* (1), 20−25.
(53) van den Bleek, C. M.; van der Wiele, K.; van den Berg, P. J. The Effect of Dilution on the Degree of Conversion in Fixed Bed Catalytic Reactors. *Chem. Eng. Sci.* **1969**, *24* (4), 681−694.
(54) Kurtz, M.; Strunk, J.; Hinrichsen, O.; Muhler, M.; Fink, K.; Meyer, B.; Wöll, C. Active Sites on Oxide Surfaces: ZnO-Catalyzed Synthesis of Methanol from CO and H_2. *Angew. Chem., Int. Ed.* **2005**, *44* (18), 2790−2794.
(55) Wilmer, H.; Kurtz, M.; Klementiev, K. V.; Tkachenko, O. P.; Grünert, W.; Hinrichsen, O.; Birkner, A.; Rabe, S.; Merz, K.; Driess, M.; Wöll, C.; Muhler, M. Methanol Synthesis over ZnO: A Structure-Sensitive Reaction? *Phys. Chem. Chem. Phys.* **2003**, *5* (20), 4736−4742.
(56) Lunkenbein, T.; Schumann, J.; Behrens, M.; Schlögl, R.; Willinger, M. G. Formation of a ZnO Overlayer in Industrial Cu/ZnO/Al_2O_3 Catalysts Induced by Strong Metal-Support Interactions. *Angew. Chem., Int. Ed.* **2015**, *54* (15), 4544−4548.
(57) Byrne, D.; Fath Allah, R.; Ben, T.; Gonzalez Robledo, D.; Twamley, B.; Henry, M. O.; McGlynn, E. Study of Morphological and Related Properties of Aligned Zinc Oxide Nanorods Grown by Vapor Phase Transport on Chemical Bath Deposited Buffer Layers. *Cryst. Growth Des.* **2011**, *11* (12), 5378−5386.
(58) Yu, J.; Yang, M.; Zhang, J.; Ge, Q.; Zimina, A.; Pruessmann, T.; Zheng, L.; Grunwaldt, J.-D.; Sun, J. Stabilizing Cu^+ in Cu/SiO_2 Catalysts with a Shattuckite-like Structure Boosts CO_2 Hydrogenation into Methanol. *ACS Catal.* **2020**, *10*, 14694−14706.
(59) Wang, L.; Lu, X.; Huang, Y. Determination of Zn Distribution and Speciation in Basic Oxygen Furnace Sludge by Synchrotron Radiation Induced μ-XRF and μ-XANES Microspectroscopy. *X-Ray Spectrom.* **2013**, *42* (6), 423−428.
(60) Rose, J.; Moulin, I.; Masion, A.; Bertsch, P. M.; Wiesner, M. R.; Bottero, J.-Y.; Mosnier, F.; Haehnel, C. X-Ray Absorption Spectroscopy Study of Immobilization Processes for Heavy Metals in Calcium Silicate Hydrates. 2. Zinc. *Langmuir* **2001**, *17* (12), 3658−3665.
(61) Veiga, J. P.; Figueiredo, M. O. A XANES Study on the Structural Role of Zinc in Ancient Tile Glazes of Portuguese Origin. *X-Ray Spectrom.* **2008**, *37* (4), 458−461.
(62) Takesue, M.; Hayashi, H.; Smith, R. L., Jr. Thermal and Chemical Methods for Producing Zinc Silicate (Willemite): A Review. *Prog. Cryst. Growth Charact. Mater.* **2009**, *55* (3−4), 98−124.
(63) van den Berg, M. W. E.; Polarz, S.; Tkachenko, O. P.; Kähler, K.; Muhler, M.; Grünert, W. Dynamical Changes in the Cu-ZnO_x Interaction Observed in a Model Methanol Synthesis Catalyst. *Catal. Lett.* **2009**, *128* (1−2), 49−56.
(64) Studt, F.; Behrens, M.; Kunkes, E. L.; Thomas, N.; Zander, S.; Tarasov, A.; Schumann, J.; Frei, E.; Varley, J. B.; Abild-Pedersen, F.; Nørskov, J. K.; Schlögl, R. The Mechanism of CO and CO_2 Hydrogenation to Methanol over Cu-Based Catalysts. *ChemCatChem.* **2015**, *7* (7), 1105−1111.
(65) Okamoto, H. Supplemental Literature Review of Binary Phase Diagrams: Ag-Ni, Ag-Zr, Au-Bi, B-Ni, Co-Sb, Cu-Mn, Cu-Si, Cu-Zn, Fe-Zr, Li-Sb, Mg-Pu, and Si-Zr. *J. Phase Equilibria Diffus.* **2018**, *39*, 87−100.
(66) Zhou, Y.; Jin, C.; Li, Y.; Shen, W. Dynamic Behavior of Metal Nanoparticles for Catalysis. *Nano Today* **2018**, *20*, 101−120.
(67) Spencer, M. S. α-Brass Formation in Copper/Zinc Oxide Catalysts: II. Diffusion of Zinc in Copper and α-Brass under Reaction Conditions. *Surf. Sci.* **1987**, *192* (2−3), 329−335.
(68) Guisbiers, G.; Buchaillot, L. Size and Shape Effects on Creep and Diffusion at the Nanoscale. *Nanotechnology* **2008**, *19* (43), 435701.
(69) Guisbiers, G.; Kazan, M.; van Overschelde, O.; Wautelet, M.; Pereira, S. Mechanical and Thermal Properties of Metallic and Semiconductive Nanostructures. *J. Phys. Chem. C* **2008**, *112* (11), 4097−4103.

https://doi.org/10.1021/acscatal.1c05101
ACS Catal. 2022, 12, 6628−6639